Binary Fe-based amorphous wires prepared by the melt-extraction method

WEIMING YANG[a], WENYU LI[a], CHAO WAN[a], JUNTAO HUO[b,*], BINGZHUO LIU[c], BAOLONG SHEN[d], HAISHUN LIU[a,*], AKIHISA INOUE[e]

[a]*State Key Laboratory for Geomechanics and Deep Underground Engineering, School of Mechanics and Civil Engineering, China University of Mining and Technology, Xuzhou 221116, People's Republic of China*

[b]*Key Laboratory of Magnetic Materials and Devices, Ningbo Institute of Materials Technology & Engineering, Chinese Academy of Sciences, Ningbo 315201, People's Republic of China*

[c]*Department of Electrical and Electronic Engineering, The University of Melbourne, Victoria 3010, Australia*

[d]*School of Materials Science and Engineering, Southeast University, Nanjing 211189, People's Republic of China*

[e]*International Institute of Green Materials, Josai International University, Togane, 283-8555, Japan*

Fe-based amorphous wires are promising in small-size functional components and devices due to their high thermal conductivity and soft magnetic properties. However, it is a great challenge to fabricate binary Fe-based amorphous wires through traditional preparation techniques. In this letter, $Fe_{91}Zr_9$ amorphous wires with a smooth surface and negligible deviation in diameter were firstly prepared using the melt-extraction method. Their microstructure, magnetic properties and tensile strength were evaluated. This work is expected to promote the application of Fe-based amorphous alloys in flexible sensors, wearables and magnetic refrigerants.

(Received July 28, 2019; accepted June 16, 2020)

Keywords: Amorphous materials, Magnetic properties, Microstructure

1. Introduction

Fe-based amorphous alloys (FAAs) at micrometer or sub-micrometer scale have great potentiality in the application of small-size components, micro-electro-mechanical systems and bio-sensors for their high thermal conductivity and soft magnetic properties [1-5]. Conventionally, Fe-based amorphous wires (FAW) are produced by glass-coated melt spinning method [6-9], accompanied with the following disadvantages [7, 10]: (1) the diameter of FAW is limited below 20 μm because of the slow cooling rate; (2) the spun alloys must possess nearly the same melting temperature as the flow point of the coating glasses; and (3) the coating glass must be removed by dissolving in hydrofluoric acid. Up to now, almost all the binary FAAs, such as Fe-Zr, Fe-P, Fe-Hf, Fe-C and Fe-Sc, fabricated by conventional fast cooling techniques are ribbons or powders [11-15]; these shapes significantly limits their commercial proliferation, confronting great challenges in the evaluation of tensile properties of these FAAs. It is necessary to develop a technique for the fabrication of binary FAWs with a circular cross-section. More recently, Co-Fe-Cr-Si-B amorphous wires was reported prepared by melt-extraction method [16-17], indicating the possibility of producing amorphous wires with small glass-forming ability and supercooled liquid region. This method is also easily to be controlled and convenient for the fabricating the continuous amorphous wires with circular cross section, smooth surface and negligible deviation in diameter.

In this letter, we attempted to examine the possibility of fabricating amorphous wire in the binary Fe-Zr system in an optimum melt extraction condition by means of the melt-extraction method. The aim of this letter is to outline the melt-extraction method for binary FAW, and report its shape, size and mechanical properties.

2. Experimental

Ingots with nominal composition of $Fe_{91}Zr_9$ (at. %) were prepared by arc melting pure elements (99.99 wt. %) in an argon atmosphere. To ensure homogeneous, every ingot was remelted five times. Amorphous ribbons with an approximate width of 1.0 mm and thickness of ~30 μm were prepared by single roller melt spinning method with a surface speed of 40 m/s under an argon atmosphere. Amorphous microwires are fabricated successfully by the melt-extraction method as shown in Fig. 1. The feed rate of the sample holder was set to be 90 μm^{-1}. The temperature was determined by a Raytek integrated ratio infrared thermometer and the sample was heated up to the temperature about 50 K above the melt point. The edge

angle of the Mo wheel was fixed at an angle of 60°. The circumferential velocity of the Mo wheel was 30 m/s. By moving up the sample holder toward the Mo wheel the melt was extracted sideways under a high purity argon atmosphere, and formed a fine, rapidly cooled circular wire with a high surface-to-volume ratio. The amorphous nature of samples was certified by X-ray diffraction (XRD, D8-Discover, Brucker) with a Cu Kα radiation, and thermal analysis was performed by a differential scanning calorimeter (DSC, 404 F3, Netsch) with a heating rate of 40 K/min. Temperature and field dependences of the DC magnetization were measured in the temperature range of 10 – 300 K under a field of 0.02 T using the magnetic property measurement system. Tensile tests were performed on the microcomputer control electron universal testing machine. Hardness tests and Vickers indentation tests of wires after inlaying and polishing were performed on digital durometer. The tensile fracture and Vickers indentation morphology were examined using a scanning electron microscope (SEM, FEG 250).

3. Results and discussion

Fig. 2 shows a typical SEM micrograph of the peripheral surface of $Fe_{91}Zr_9$ amorphous wire. Deviation in the wire diameter is about 10 % for the wire approximately 30 μm in diameter and it tends to decrease with decreasing wire diameter. Thus, the FAW produced by this technique possess a good uniformity of shape, indicating the high stability of the melts on rotating Mo wheel.

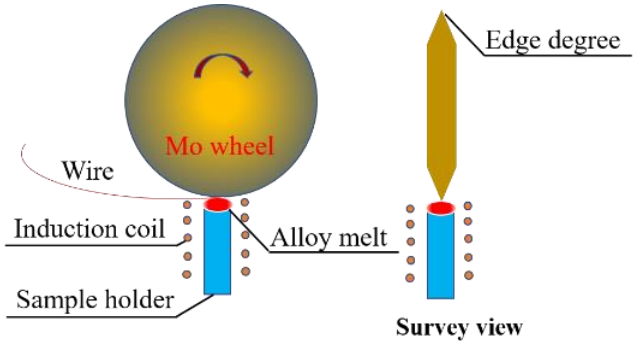

Fig. 1. Schematic illustration for a melt-extraction technique used in the present study (color online)

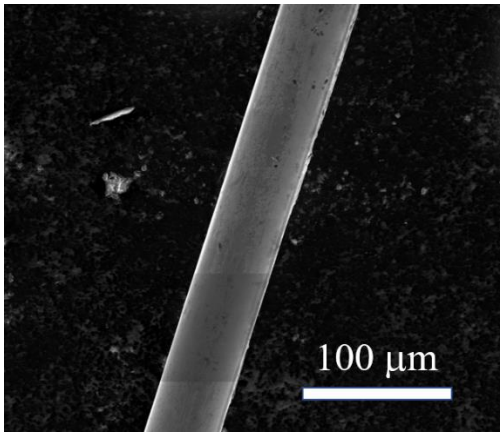

Fig. 2. SEM micrograph showing the peripheral surface of as-extracted $Fe_{91}Zr_9$ amorphous wire

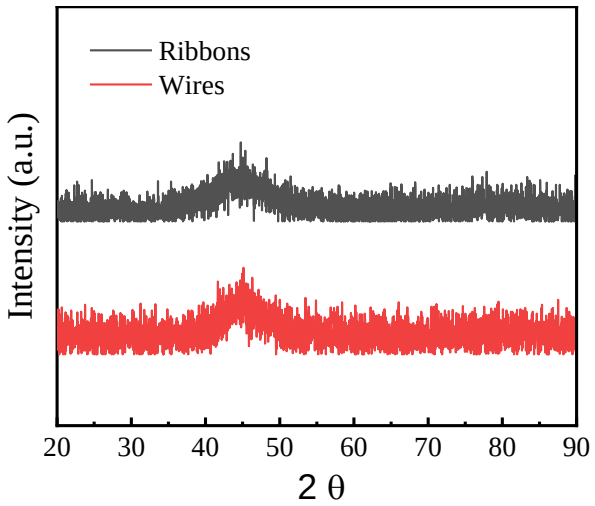

Fig. 3. XRD patterns of $Fe_{91}Zr_9$ amorphous ribbon and wire (color online)

Fig. 3 shows XRD patterns of as-quenched $Fe_{91}Zr_9$ ribbon and as-extracted wire. The XRD patterns show only broad peaks, and no obvious crystalline peaks can be detected, indicating the amorphous structures of the ribbon and wire. DSC curves of $Fe_{91}Zr_9$ alloy ribbon and wire are shown in Fig. 4. No glass transition is recognized, while obvious crystallization exothermic peaks are observed, consistent with the results obtained by X-ray diffraction. The sharp crystallization event also confirms the formation of an amorphous phase for the wire.

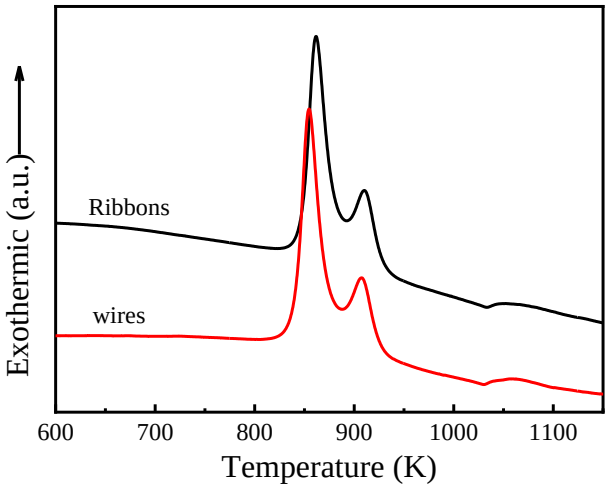

Fig. 4. DSC curves for $Fe_{91}Zr_9$ amorphous ribbon and wire (color online)

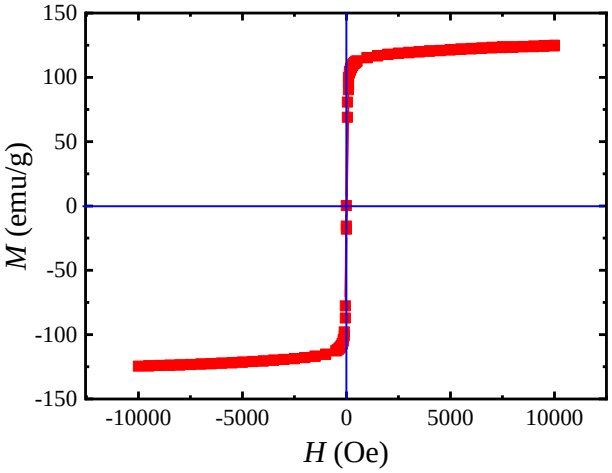

Fig. 5. Hysteresis loops for $Fe_{91}Zr_9$ amorphous wire under 5 T at 10 K (color online)

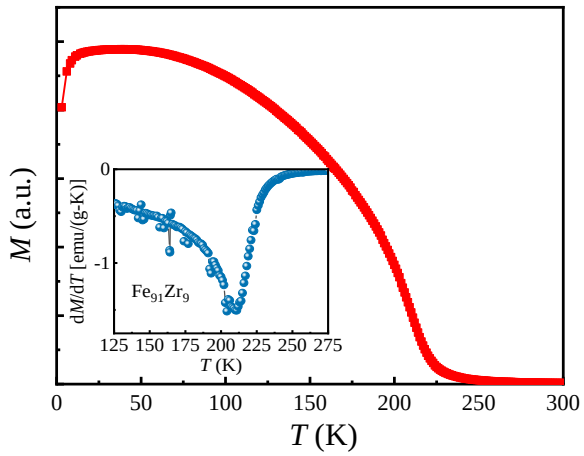

Fig. 6. Temperature dependence of magnetization under a magnetic field of 200 Oe. The inset displays the thermal derivative of the magnetization data as a function of temperature (color online)

Fig. 5 shows the magnetic hysteresis loop for $Fe_{91}Zr_9$ amorphous wire at 10 K. The wire exhibits the saturation magnetization (M_s) of 123 emu/g. The temperature dependence of magnetization is also presented in Fig. 6. The Curie temperature (T_c) of the amorphous wire is about 210 K. The M_s and T_c are determined by the total magnetic moment in the amorphous structure [18]; the atomic magnetic moment is assumed to be dependent on the number of the nearest-neighbor Fe atoms and Fe-Zr interaction [19, 20]. It should be noted that as shown in Fig. 6, the magnetization decreases with temperatures decreasing below 10 K. It is attributed to the fact that the higher Zr content in the present alloy has enhanced the ferromagnetic interaction [21] and spin glass behavior [22].

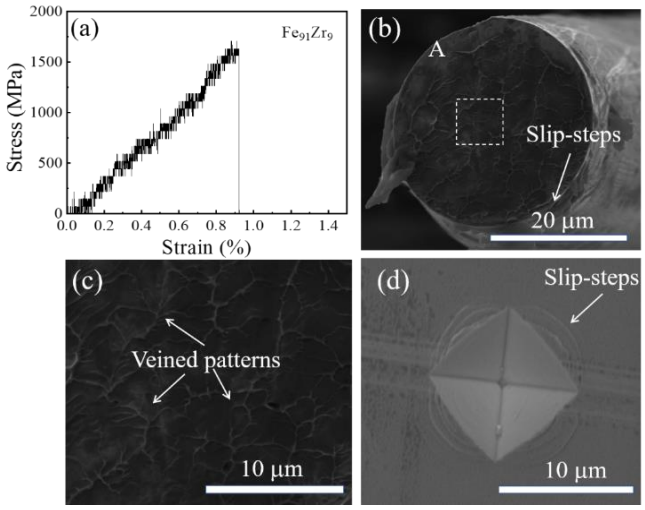

Fig. 7. (a) Tensile stress-strain curve for $Fe_{91}Zr_9$ amorphous wire. (b) SEM image of the fracture morphology showing an inclined fracture. (c) Magnified SEM image taken from the rectangular region in (b). (d) Vickers indentation SEM image of $Fe_{91}Zr_9$ amorphous wire

Tensile stress-strain curve of $Fe_{91}Zr_9$ amorphous wire at room temperature is shown in Fig. 7 (a). The initial strain rate was 0.2 mm/min. No appreciable plastic strain is recognized, indicating that the sample fractured by a catastrophic brittle mode. The fracture strength σ_f is 1620±50 MPa. The SEM images revealing the tensile fracture surface morphology are shown in Fig. 7 (b) and (c). A number of shear bands are observed in the lateral surface region, and distinct vein pattern is also observed on the fracture surface, indicating that the shear bands generated even in the elastic strain region. The shear type fracture mode implies that the tensile failure is controlled by the normal stress and the shear stress [16]. The Vickers hardness is 726 kg/mm^2 for the as-extracted $Fe_{91}Zr_9$ amorphous wire. A SEM image revealing the slip markings around the hardness indentation trace is shown

in Fig. 7 (d). A number of slip-steps markings are observed in the vicinity of the indentation trace. The absence of obvious crack and the presence of slip-steps markings indicate that the wire is ductile adequate to prevent catastrophic fracture under loading. In the following, more binary Fe-based amorphous wires and their properties need to be further explored in the future.

4. Conclusion

This study shows the fabrication process of $Fe_{91}Zr_9$ amorphous wire by using a novel and facile method via melt-extraction. The dimensional accuracy of the produced wires and the appropriateness of the post-characterization methods, i.e. structural, mechanical, thermal, magnetic properties investigations, for the amorphous wire confirms the production technique's suitability to be used in different fields. This work is expected to promote the application of Fe-based amorphous alloys in flexible sensors, wearables and magnetic refrigerants.

Acknowledgements

This work was supported by the National Natural Science Foundation of China (No. 51631003 and 51871237) and Xuzhou Key Research & Development Program (KC17015).

References

[1] Y. Wu, Y. Liu, Y. Zhou, Q. Man, C. Hu, W. Asghar et al., Science Robotics **3**, eaat0429 (2018).
[2] A. Grujic, T. Zak, V. Cosovic et al., Optoelectron Adv. Mat. **3**, 477 (2009).
[3] S. A. Ciureanu, Optoelectron Adv. Mat. **4**, 714 (2010).
[4] Y. Hu, M. X. Pan, L. Liu, Y. H. Zhao, W. H. Wang, Mater. Lett. **57**, 2698-701 (2003).
[5] Y. Huang, Y. Guo, H. Fan, J. Shen, Mater. Lett. **89**, 229-32 (2012).
[6] Y. Zhao, H. Li, H. Hao, M. Li, Y. Zhang, P. Liaw, Rev. Sci. Instrum. **84**, 075102 (2013).
[7] A. Zhukov, M. Vázquez, J. Velázquez, A. Hernando, V. Larin, J. Magn. Magn. Mater. **170**, 323-30 (1997).
[8] V. Manov, P. Popel, E. Brook-Levinson, V. Molokanov, M. Calvo-Dahlborg, U. Dahlborg et al., Mater. Sci. Eng. A **304**, 54 (2001).
[9] A. Zhukov, Appl. Phys. Lett. **78**, 3106-8 (2001).
[10] T. Masumoto, I. Ohnaka, A. Inoue, M. Hagiwara, Scr. Metall. **15**, 293-6 (1981).
[11] F. Luborsky, H. Liebermann, Appl. Phys. Lett. **33**, 233-4 (1978).
[12] H. Hiroyoshi, K. Fukamichi, J. App. Phys. **53**, 2226-8 (1982).
[13] R. Gopalan, Y. Chen, T. Ohkubo, K. Hono, Scr. Mater. **61**, 544-7 (2009).
[14] A. Inoue, J. Saida, T. Masumoto, Mater. Trans. JIM. **30**, 291-9 (1989).
[15] Y. Fang, Z. Yu, G. Peng, T. Feng, J. Non-Cryst. Solid. 505, 211-214 (2019).
[16] W. Liao, Z. Chen, M. Li, J. He, Y. Zhang, Mater. Lett. **97**, 195-7 (2013).
[17] A. Inoue, A. Katsuya, K. Amiya, T. Masumoto, Mater. Trans. JIM. **36**, 802-9 (1995).
[18] K. Kim, S. Min, S. Yu, S. Oh, Y. Kim, K. Kim, J. Magn. Magn. Mater. **304**, e642-e4 (2006).
[19] W. W. Heisenberg, Z. Phys. **49**, 619 (1928).
[20] M. Kim, S. H. Lim, J. Magn. Magn. Mater. **476**, 559 (2019).
[21] D. Mishra, M. Gurram, A. Reddy, A. Perumal, P. Saravanan, A. Srinivasan, Mater. Sci. Eng. B **175**, 253 (2010).
[22] J. Li, L. Xue, W. Yang, C. Yuan, J. Huo, B. Shen, Intermetallics **96**, 90 (2018).

*Corresponding authors: huojuntao@nimte.ac.cn
liuhaishun@cumt.edu.cn